Sensors and Actuators A 293 (2019) 189–199

Contents lists available at ScienceDirect

Sensors and Actuators A: Physical

journal homepage: www.elsevier.com/locate/sna

Coupling pulse eddy current sensor for deeper defects NDT

Lian Xie[a], Bin Gao[a,*], G.Y. Tian[a,b], Jidong Tan[c], Bo Feng[d], Ying Yin[e]

[a] School of Automation, University of Electronic Science and Technology of China, China
[b] School of Electrical and Electronic Engineering, Newcastle University, England, UK
[c] China Special Equipment Inspection and Research Institute, China
[d] Instituto de Telecomunicações, Universidade de Lisboa, Portugal
[e] Sichuan Special Equipment Inspection Institute, China

ARTICLE INFO

Article history:
Received 22 December 2018
Received in revised form 5 March 2019
Accepted 19 March 2019
Available online 30 April 2019

Keywords:
Pulsed eddy current
Weak coupling
Subsurface defects
Nondestructive testing

ABSTRACT

Deep defect detection for ferromagnetic materials is a challenging task for Eddy Current testing (ECT) due to the skin effect of the low penetration depth. Pulsed Eddy Current testing (PECT) is a potential and effective method for detecting deep subsurface defects as it can obtain multiple depth information owing to its wide spectrum range. A novel weak coupling sensing structure of pulsed eddy current is proposed. In particular, the structure improves the ratio of the indirect coupling energy by reducing the direct coupling energy between the excitation and the detection coils. It obviously improves the ability to detect deep subsurface defects of ferromagnetic materials. The principle of penetration and the analysis of its equivalent circuit are presented. In addition, both experiments and simulations on different defects detection have been studied. The results have confirmed that all types of defects can be detected and it has shown the relatively monotonic linear relationships and reliability.

1. Introduction

Eddy Current testing (ECT) technology is a nondestructive testing (NDT) method to detect the surface or near-surface defects for conductive materials. As a branch of electromagnetic NDT, the eddy current induced by the excitation coil connected to alternating current will carry the information of the specimen according to the Faraday's law from electromagnetic induction. ECT has several advantages: 1) non-contact detection can penetrate coating layer without coupling medium [1]; 2) defects can be detected under the condition of high temperature and the probe of ECT can be made into various shapes in order to adapt with different objects; 3) higher sensitivity to near-surface defects [2,3]. Due to its superiority and easily automation, it is widely applied in NDT field [4]. The research direction on the design of ECT system includes several aspects: the optimization of the sensor structure as well as the excitation parameters [5–7]. These include the shape of excitation coil [8,9], pulse or coding excitation mode. In addition, the differential probe for ECT has been developed to improve the detection sensitivity [10–13]. In addition, the design of the probe array has been expanded [14–17] for achieving the scanning image [18]. Notwithstanding above, the excitation mode is considered to improve the detectability, these include the pulse modulation signal [19] and the triangle wave modulation signal [20]. In particular, ECT is generally applied to the detection of the surface and subsurface defects [21,22].

However, the material properties significantly affect the depth of the eddy current penetration since the detection of common ECT is limited by the skin effect [23]. Nevertheless, the detection of the deeper defects has made achievements. DF He et al. [24] took advantage of anisotropic magnetoresistance (AMR) sensor, and achieved the defects detection with the depth of 15 *mm* on aluminum alloy specimen. Hesse O et al. [25] studied the influence of different magnetic sensors, e.g. AMR, induction coil and giant magnetoresistance (GMR), on the detection sensitivity under the low frequency eddy current testing. The induction coil allows low frequency eddy current detection at high temperature with a high performance. Hohmann R et al. [26] developed the superconducting interference devices (SQUID) robot system which can penetrate 25% of the internal defects of the wall thickness. Compared with inductive sensors, SQUID can identify smaller defects. Kreutzbruck M et al. [27] studied the deeper defect detection of fluxgate sensor under the low excitation frequency. The system has a wide bandwidth and can detect deep cracks between 2 *mm* and 25 *mm* in aluminum specimens. Kang H L et al. [28] investigated the equivalent impedance of the eddy current, and the frequency of the excitation is reduced to 0.1 *Hz*-1 *Hz* simultaneously. As a result, the defects under 4 *mm* depth can be detected in the shaped steel com-

* Corresponding author.
E-mail address: bin.gao@uestc.edu.cn (B. Gao).

https://doi.org/10.1016/j.sna.2019.03.029
0924-4247/

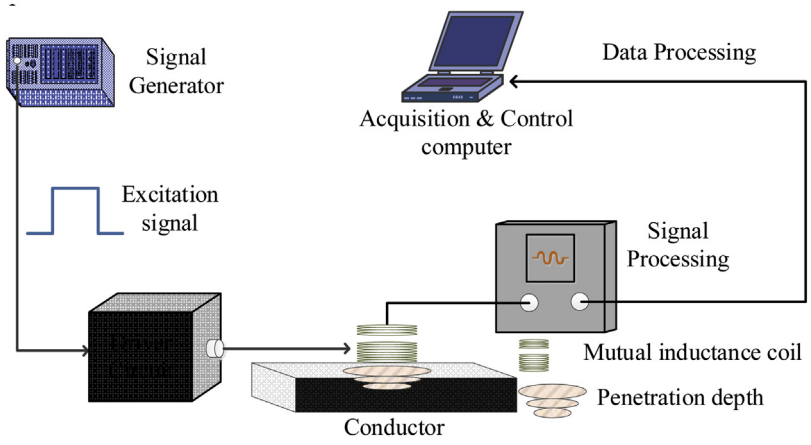

Fig. 1. The proposed schematic of the PEC system.

ponent. Janousek L et al. [29] adopted an exciting phase difference to gain deeper penetration, and the advantage of high frequency is maintained at the same time. Thus, the defects with a depth of 5 *mm* in aluminum alloy can be detected.

Different from the common ECT methods, pulsed eddy current (PEC) which retains a certain range of continuous multi-frequency spectrum carries wide information of the specimen on account of the different penetration depth [30]. The research on deep defects detection verifies the diversity of the PEC spectrum. Angani C S et al. [31] designed a differential sensor to improve the signal-to-noise ratio, and investigated the feature of power spectral density. Kiwa T et al. [18] proposed the Fourier transform method to obtain the response of the intrinsic frequency, and the cross-sectional images of the samples can be directly constructed. At the same time, the defects at a depth of 2 *mm* can be detected. Yang G et al. [32] generates transient magnetic field by pulsed excitation of planar multi-wire multi-layer coils for small cracks detection of using GMR sensor. In order to effectively increase the penetration depth of pulsed eddy current signal, a method of increasing the excitation current was proposed to detect crack defects in 10 *mm* thick steel plate [33]. Park D G et al. [34] developed a differential probe for PEC system to detect subsurface cracks in SS304 stainless steel tubes. Lebrun B et al. [35] detected cracks in AU4G structure by step current excitation to reduce the direct coupling phenomenon of coils based on pulsed eddy current detection method. He Y et al. [36] studied PEC imaging and spectrum analysis based on magnetic induction direction of rectangular excitation coil, and showed that the special characteristics of magnetic induction direction were still effective for detecting subsurface defects in the presence of sample edge effect. Spectrum analysis was helpful for defect classification. Abidin I Z et al. [37] studied the application of pulsed eddy current detection method in the depth detection of defects in layered structures. It shows that by changing the pulse width properly, the influence of appropriate frequency components on defect detection and depth estimation can be reduced or enhanced. Thus, ECT demonstrates the ability to detect deeper defects in non-ferromagnetic materials.

However, deeper defects detection by ECT still faces the issues of the low penetration depth and skin effect for ferromagnetic material. Specifically, since distribution of the electromagnetic field is a key point for ECT, several impact factors have to be considered:1) the effective depth and the range of the sensor detection; 2) the relative position of the defect and the sensitivity from the sensor influences; 3) the ratio of direct coupling energy to indirect coupling energy affects the sensitivity of the response signal.

In this paper, a novel mutual inductance PEC sensor structure is proposed with high permeability and energy ratio. Different from traditional eddy current detection methods, the induction coil with a wide frequency response range is selected as the detection sensor in this paper, which is based on the characteristics of the pulse with rich spectrum information. In particular, the structure comprises the electromagnetic mechanism of utilizing the weak coupling sensing structure for interpreting the difference between air magnetoresistance and specimen magnetoresistance. This mainly combines the characteristics of weak coupling transmission where it attenuates the direct coupling energy. On the other hand, the low-frequency components, which has stronger penetration ability, can dig out the subsurface defect information while the energy attenuated by the air magnetoresistance is smaller. It improves the proportion of the low frequency indirect coupling energy that can carry deep defect information from the signal. Thus, the proposed sensor enables to perform higher detection sensitivity for the deep subsurface defects by adjusting the ratio of the indirect coupling energy to direct coupling energy. Furthermore, the sensitivity of deep defect detection is improved, and the deep defect detection of ferromagnetic materials and non-ferromagnetic materials is realized. The reliability of the probe structure is verified on both non- ferromagnetic and ferromagnetic specimens.

The rest of this paper is organized as follows. In Section 2, the transmission theory based on the magnetic coupling mutual inductance model and the theoretical analysis based on PEC detection are discussed. A new structure of pulsed eddy current sensor is proposed. Section 3 conducts a simulation of the parameters influence on mutual inductance in conjunction with analytical model and optimization design technique. Then, an experimental setup is constructed to verify the model. In Section 4, a conclusion is given.

2. Methodology

The new mutual inductance PEC system is proposed and illustrated in Fig.1. Specifically, the sensor is mainly composed of two sets of coils. The exciting coil is placed on the upper surface of the material, and the detection coil is placed above the excitation coil. When the excited pulse signal drives to the coil, an alternating magnetic field is generated, and the eddy current will be induced in the specimen. In addition, the interruption caused by the defect in magnetic field can be detected by the pick- up coil.

Different from general PEC system, the proposed probe structure has an insight to the attenuation of the direct energy to increase the ratio of the indirect coupling energy. Meanwhile, PEC has rich spectrum characteristics which can increase the power of the induced eddy current compared with sinusoidal eddy current with single frequency. It overcomes the limitation of the traditional way by

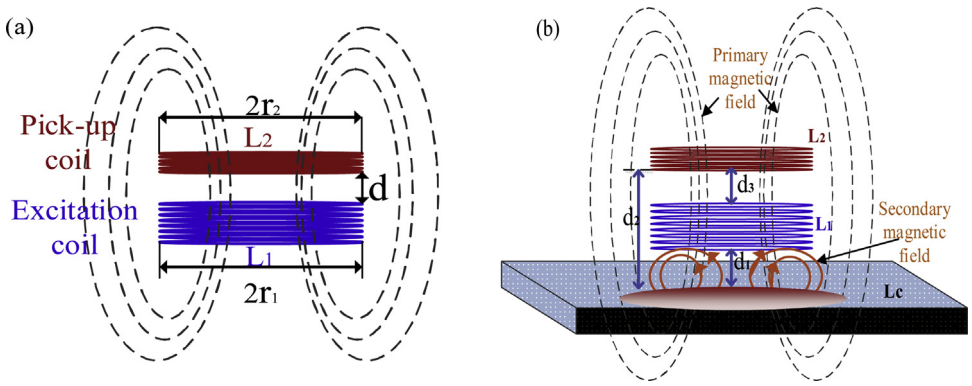

Fig. 2. Structure of the proposed PEC probe. (a) Magnetically coupled inductive wireless power transmission system without the testing sample, (b) Magnetic coupling-mutual inductance model with testing sample.

inserting a magnetic core to increase the power of the induced eddy current. In addition, this schematic enables the eddy current to reach higher penetration depth. The following section describes the physical mechanism of the proposed structure.

2.1. Theory of the penetration principle and energy attenuation in PEC

Conductivity and permeability are two important factors that affect eddy current penetration and eddy current distribution density. The standard penetration depth formula of the eddy current is shown as:

$$\delta = \frac{1}{\sqrt{\pi f \mu_0 \mu_r \sigma}} \tag{1}$$

where f is the excitation frequency, μ_0 is the permeability of vacuum, μ_r is the relative permeability, and σ is the conductivity.

The principle of the detection penetration depth of the single frequency eddy current can be applied to the pulsed eddy current. The amplitude of a pulse square wave is V, the period is T, the pulse width is Δ, and the Fourier series of pulse excitation can be expressed as:

$$f(t) = A_0 + \sum_{n=1}^{\infty} A_n \sin(n\omega t + \varphi) \tag{2}$$

where ω is the fundamental angular frequency and φ is the phase. The amplitude of the nth harmonic is expressed as:

$$A_n = \frac{2V}{n\pi}\left|\sin\left(\frac{n\pi\Delta}{T}\right)\right| \tag{3}$$

From Eq. (3), the magnitude of the harmonic is related to the ratio of $\frac{\Delta}{T}$. When the duty cycle of the excitation signal is 50%, that is $T = 2\ \Delta$, the fundamental frequency and harmonic frequency can be expressed as EqS. (4) and (5), respectively.

$$\omega = 2\pi f = 2\pi\frac{1}{T} = \frac{\pi}{\Delta} \tag{4}$$

$$\omega_n = n\omega_0 = n\frac{\pi}{\Delta},\ n = 1, 3, 5, 7\cdots, \infty \tag{5}$$

Thus, the penetration depth of nth harmonics can be converted to Eq. (6).

$$\delta = \sqrt{\frac{2\Delta}{n\pi\mu_0\mu_r\sigma}},\ n = 1, 3, 5, 7\cdots, \infty \tag{6}$$

From Eq. (6), the penetration depth can be increased by choosing a lower impulse frequency and increasing the duty cycle.

Simultaneously, the eddy current density of the nth harmonic in the axial direction at the depth x of the specimen can be calculated by Eq. (7).

$$J(x, n) = J_0 e^{-x/\delta} = J_0 e^{-\sqrt{\frac{n\pi\mu_0\mu_r\sigma}{2\Delta}}x},\ n = 1, 3, 5, 7\cdots, \infty \tag{7}$$

$$\theta(x, n) = -\sqrt{\frac{n\pi\mu_0\mu_r\sigma}{2\Delta}}x,\ n = 1, 3, 5, 7\cdots, \infty \tag{8}$$

where J_0 is the eddy current density at the surface of the specimen in the axial direction of the excitation coil, $\theta(x, n)$ represents the change of phase as shown in Eq. (8).

According to Eq. (7) and (8), increasing the pulse duty cycle reduces the phase angle of the signal, slows down the eddy distribution density and reduces the sensitivity. In addition, the energy attenuation of the high-frequency component is faster than that of the low frequency component.

2.2. Energy transfer theory of the mutual inductance coil

Fig. 2(a) and (b) show the magnetic coupling mutual inductance model with and without samples, respectively.

The magnetic coupling-mutual inductance coupling model is shown in Fig. 2. In particular, the key parameter of the circuit model is the coupling coefficient which is related to the turns of the driver coil N_1, the turns of the pickup coil N_2, the radius of the wire r_1, r_2, and the equivalent distance between two coils d. The equivalent circuit models are shown in Fig. 3(a) and (b), respectively.

According to mutual inductance theory and Kirchhoff's law, the output voltage of the coil in Fig. 3(a) can be expressed as:

$$V_{out} = -\frac{j\omega M U_i}{Z_1 Z_2 + (\omega M)^2} R_L \tag{9}$$

where Us = excitation voltage, R_L = load resistance, Z_1 = driver coil impedance, Z_2 = pickup coil impedance, R_S = signal source resistance, L_1 = driver coil inductance, L_2 = pickup coil inductance. M_0 = mutual inductance coefficient.

According to Newman formula [38], the mutual inductance coefficient of coaxial coils arranged in space can be calculated as:

$$M = \mu N_1 N_2 \frac{\sqrt{r_1 r_2}}{b}\left(\left(2 - b^2\right)K(b) - 2E(b)\right) \tag{10}$$

where $b = \sqrt{\frac{4r_1 r_2}{(r_1+r_2)^2+d^2}}$ $K(b) = \int_0^{\frac{\pi}{2}} \frac{d\theta}{\sqrt{1-b^2\sin^2\theta}}$, denotes the complete elliptic integral of the first kind, $E(b) = \int_0^{\frac{\pi}{2}} \sqrt{1-b^2\sin^2\theta}d\theta$ denotes the complete elliptic integral of the second kind. θ is the angle between the positions of two coils described in polar coordinates, and it is also the angle between the vectors of two coils. d is the equivalent distance between coils, μ is the permeability of dielectric between coils.

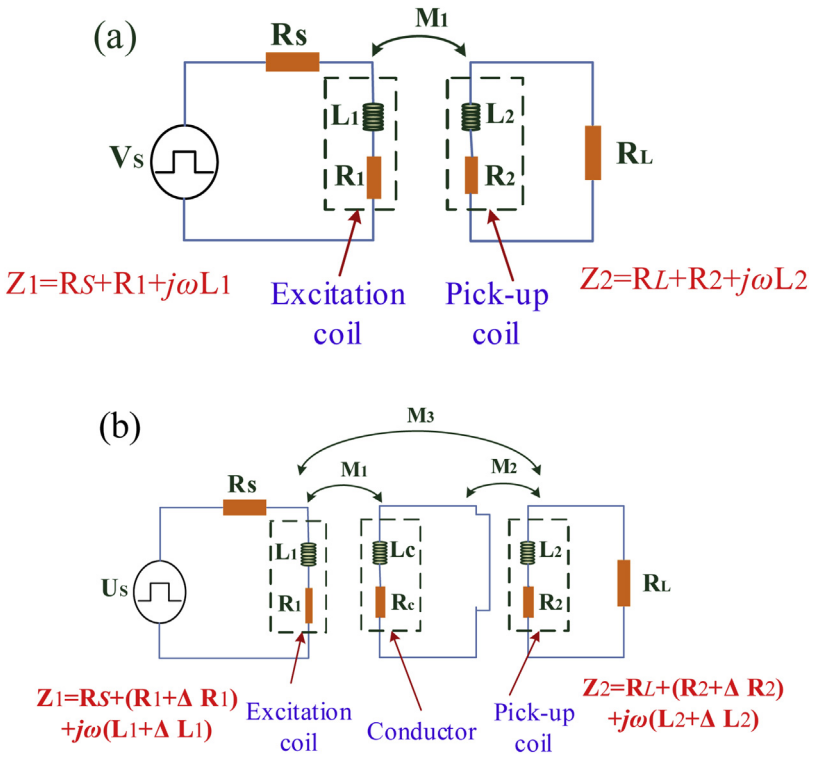

Fig. 3. Equivalent circuit of model. (a) The equivalent circuit without sample, (b) The equivalent circuit with sample.

However, the output voltage will change when a conductor exists. On account of $d_2 > d_1+d_3$, M_2 is close to zero, and the changes of the conductor impedance influence the equivalent impedance of Z_1. Thus, Formula (9) can be rewritten as:

$$V_{out}{}' = -\frac{j\omega M_3 U_S}{(Z_1 + \Delta Z_1)Z_2 + (\omega M_3)^2} R_L \tag{11}$$

According to Eq. (10), the distance of the coils can effectively adjust the transmission of the coupling energy. In the case of coaxial coils, when the distance is constant, the coupling coefficient is mainly influenced by the coil parameters. In addition, the coil spacing can be considered as the main parameter that affects the coupling coefficient. In other words, the ratio of the indirect coupling energy and the direct coupling energy can obtain the optimal detection sensitivity and detection depth by selecting the appropriate d.

3. Experiment set-up

3.1. Numerical simulation

In order to insight the detection capability of the proposed PEC sensor, several simulation and verification tests were performed. All simulation experiments were implemented by AC/DC module in COMSOL MULTIPHYSICS. A rectangular waveform with a 300 *mA* current and 10 *ms* period was used to drive the excitation coil. The specimen size is 100 *mm* × 100 *mm* × 10 *mm* and the lift-off distance is 0 *mm*. The excitation current and response signal of a descending edge of the pulsed eddy current is shown in Fig. 4.

The parameters of PEC probe are shown in Table 1. There are two kinds of specimen, i.e. aluminum alloy and 45 steel. The material properties are listed in Table 2.

The simulation analysis takes ferromagnetic material 45 steel as an example. The important parameter of the coil spacing d is optimized by 2-D axisymmetric simulation model. The defect in the model is set as 5 *mm* deep and 1 *mm* radius as shown in Fig. 5(a).

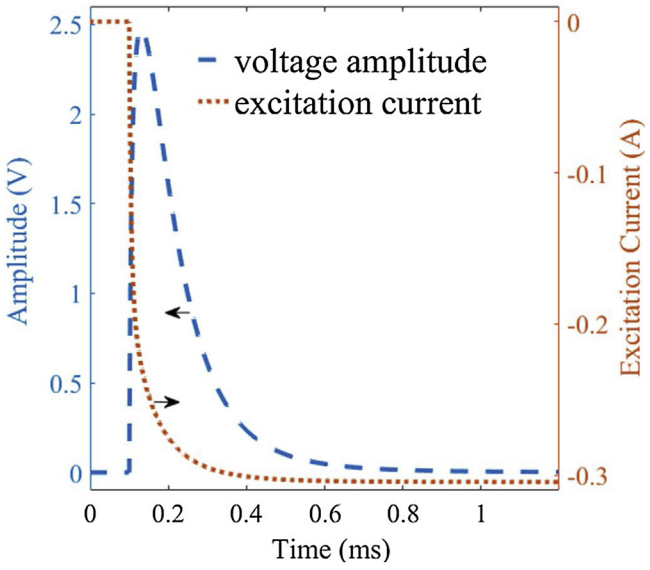

Fig. 4. Simulated signal of impulse descent edge excitation and response.

With the increase of d, the detection sensitivity increases at the first stage and then decreases. The maximum value will be obtained at d = 3 *mm*. The optimal detection sensitivity (as shown in Eq. (12)) can be obtained from Fig. 5(b).

$$Sensitivity = Max(V_{defect} - V_{defect-free}) \tag{12}$$

Additionally, the schematic diagram of 3-D simulation model of the weak coupled sensor for 45 steel is shown in Fig. 6(a). The defect length is 20 *mm* and the width is 2 *mm*. The top view of the defect is shown in Fig. 6(b). The defect depths are ranged from 2 *mm* to 8 *mm* with step of 2 *mm*, and the defect width is 2 *mm*, and the placement

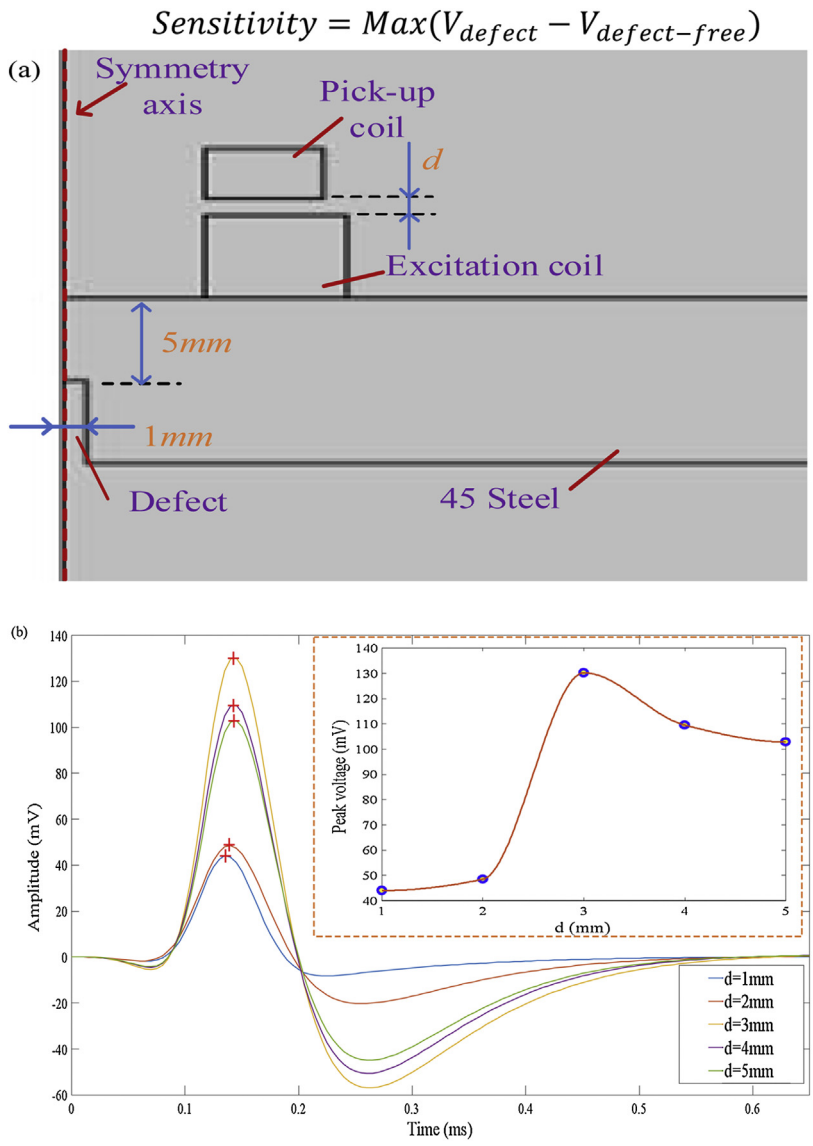

Fig. 5. The simulation optimization of coil spacing *d*. (a) Schematic representation of 2-D axisymmetric simulation model, (b) The detection sensitivity of different *d*, the inset shows the relationship between the detection sensitivity and *d*.

Table 1
Parameters of the driver and pickup coil.

Parameters	Drive coil	Pick-up coil
OD (*mm*)	24	22
ID (*mm*)	12	12
Height (*mm*)	5	3
Turns	304	600

Table 2
Properties of the specimens.

Specimen Properties	aluminum alloy	45 steel
Relative permeability μ	1	190
Electrical conductivity σ	4.84e6 [*S*/*m*]	5.5e6 [*S*/*m*]
Relative permittivity ε	1	1

of the sensor and the thickness of the tested specimen are shown in Fig. 6(c).

According to the law of electromagnetic induction, the magnetic flux directly affects the magnitude of the response signal of the pulsed eddy current. When T = 0.2 *ms*, the response signal is affected by both direct and indirect coupling energy, and the attenuation rate of response signal begins to slow down. Fig. 7 shows that the magnetic flux density of the impulse response signal at the time of 0.2 *ms*. It is close to the peak time of the impulse response signal as it can be used to characterize the distribution of the magnetic flux density in the sample at the peak time of the impulse. Simultaneously, the magnetic field generated by the excitation coil can be observed as a contrast compared with the test coil in Fig. 7. The direct coupling energy between the two coils and the indirect coupling energy through the test piece can be visually illustrated from the view of the flux density. In particular, since the air magnetoresistance is larger than that of the test piece, the direct coupling energy decays especially for the higher frequency components. As shown in Fig. 7, the proposed structure can effectively improve the ratio of the coupling energy between the detection signal and the direct coupling energy.

The magnetic flux density and induced current density are obtained to express the effective interference by defects on the induced eddy current intuitively. In the stationary time of pulse attenuation, T = 3.7 *ms* is selected, and the results are listed in Fig. 8.

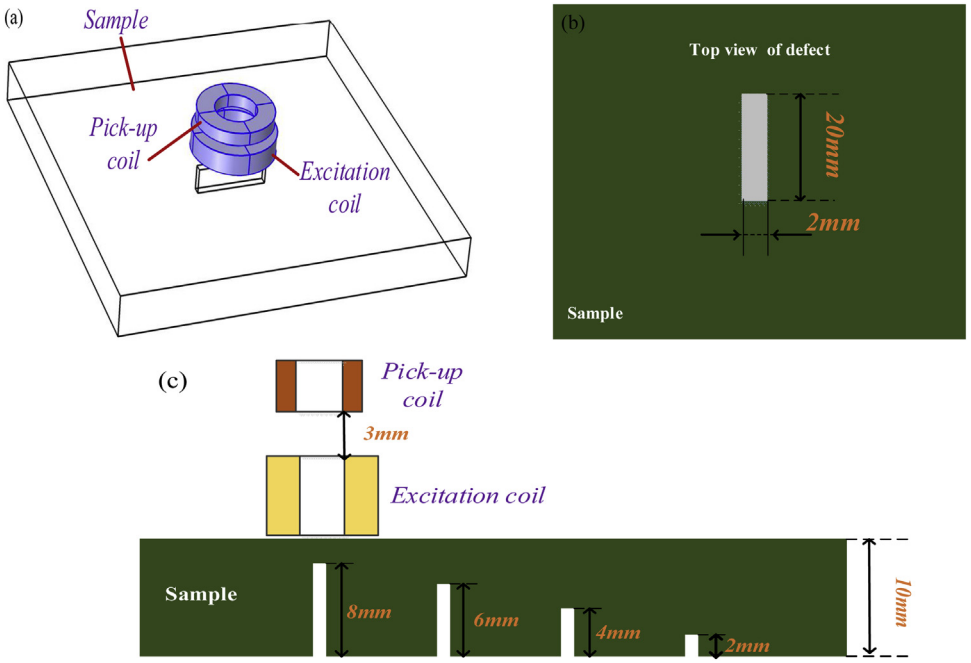

Fig. 6. Simulation schematic representation of on 45 steel and PEC probe. (a) The simulation diagram of 3-D simulation model, (b) top view of defect, (c) The structure of PEC probe and sample.

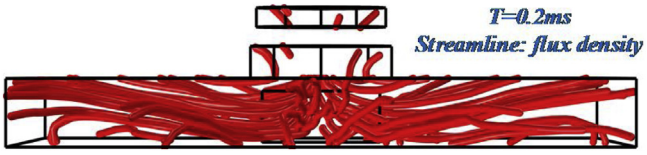

Fig. 7. The magnetic flux density distribution.

In Fig. 8, the impulse response time point of 3.7 *ms* is located in the late stage of impulse response. It can be seen from the flux density at the surface of the specimen that the effective flux density from the surface to the defect decreases with the increase of the defect depth. At the later stage of the impulse response signal, the induced eddy current disturbance caused by different depth of defects shows a great difference. This provides a reference for the selection of time domain signal of defect characterizing. With the increase of the defect depth, the flux density of effective penetration into the defect decreases, and the disturbance of induced eddy current decreases. It confirms that the sensor model can penetrate defects at 8 *mm* and interfere with the change of the induced eddy current.

In addition, the simulation response and peak values of the pulsed eddy current on aluminum alloy and 45 steel specimens are shown in Fig. 9 and Fig. 10, respectively. In the simulation of aluminum alloy specimens, the defect length is 40 *mm*, the width is 3 *mm*, the depth is 2/4/6/8 *mm*. In 45 steel, the defect length is 20 *mm*, the width is 2 *mm*, and the depth is 2/4/6/8 *mm*. The distance between the upper surface of the subsurface defect and the surface of the specimen is the depth of the defect position as expressed as D. In addition, extracting the peak characteristics of the response signal can reveal that the response signal changes monotonously with the depth of the subsurface defect.

According to the principle of electromagnetic wave transmission, the reflected magnetic field is mainly affected by the high-frequency component and the transmitted magnetic field is mainly affected by the low-frequency component. The response signal decreases with the increase of depth due to the interaction between the reflected magnetic field and the transmitted magnetic field. As a result, the amplitude of response signal decreases with the increase of defect depth as shown in Fig. 10, which is consistent with the results shown in Fig. 8.

3.2. Experimental study and validation

The experimental validation of the numerical simulation was performed with two weakly coupled hollow coils as drive and pick-up coils. The probe consists of excitation coil of 302 turns and pick-up coil of 600 turns. And the coil spacing is designed to be 3 *mm* from the simulation result. The experimental setup is shown in Fig. 11. This system mainly includes a signal generator, a DC regulated power supply, a driving circuit, a signal conditioning circuit, an oscilloscope, a new PEC probe, an XY worktable and an acquisition and control unit on computer. A pulse current signal of with amplitude of 300 *mA*, frequency of 100 *Hz* and duty cycles vary from 10% to 50% was supplied to the excitation coil. The XY worktable controls the motion of PEC probe. In addition, adding adjustable rheostat to the detection coil circuit can change the equivalent impedance of the circuit and improve the efficiency of impedance matching. The output of the pick-up coil after signal conditioning circuit is recorded from the oscilloscope. Finally, the smoothing of detection signal is processed.

The experiments were carried out on two kinds of materials, aluminum alloy and 45 steel. The information of the subsurface defects on specimen is shown in Fig. 12. The thickness of both specimens is 10 *mm*, and the depth of sub-surface defect is 2/4/6/8 *mm*. One of the differences is that the defect length of 45 steel is 20 *mm* and that of aluminum alloy is 40 *mm*. Another difference is that the defect width of 45 steel is 2 *mm* and that of aluminum alloy is 3 *mm*.

The signal was initially obtained in the defect-free region as a reference signal and the peak was used as the detection feature. In addition, the detection signals at different defect depths acquired respectively. Finally, the peak differential signals are obtained. And the results of different duty cycle are shown in Fig. 13 and Fig.14, respectively. Comparison of detection results using peak differential voltage as detection sensitivity, and the sensitivity of different duty cycle is given also.

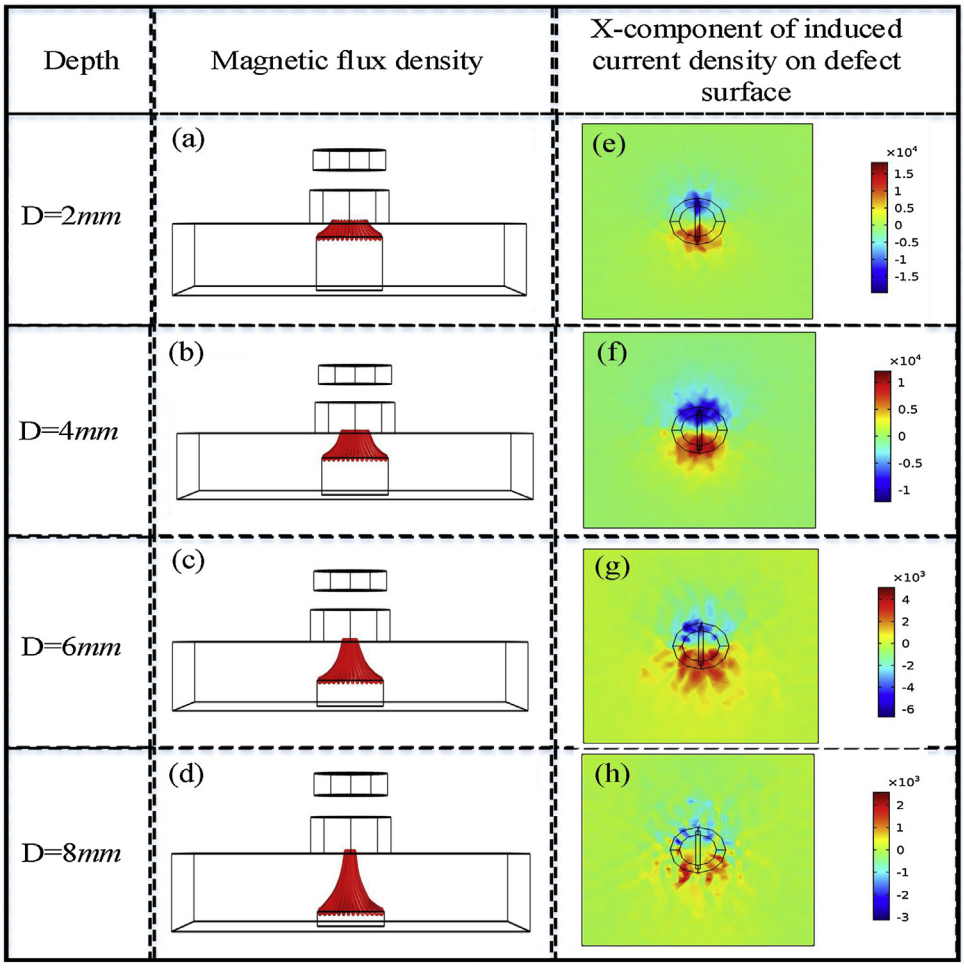

Fig. 8. The flux density and induced current on the defect ($T = 3.7$ *ms*).

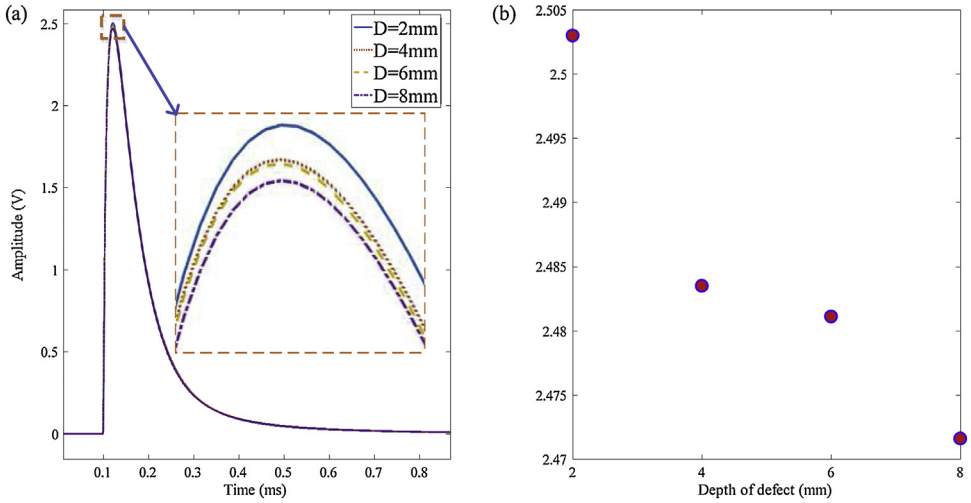

Fig. 9. The simulation response signal of different depth of defects on aluminum alloy. (a) Response signal, (b) The peak value of different defects.

Response signals with different duty cycle are shown in Fig. 13. Response signals of three different duty cycles $\tau = 10\%$, $\tau = 20\%$ and $\tau = 30\%$ are listed in Fig. 13(a)–(c), respectively. As shown in Fig. 13(d), the variation rate of deep defect is different from that of near surface defect. Peak differential voltages of $\tau = 20\%$ and $\tau = 40\%$ have similar changes for the near surface defects $D = 2$ *mm* and $D = 4$ *mm*, with strong detection ability for the near surface defects. For deep defect $D = 6$ *mm* and $D = 8$ *mm*, peak differential voltages of $\tau = 20\%$ and $\tau = 30\%$ have similar changes, and the maximum sensitivity is obtained at $\tau = 40\%$. In fact, the energy distribution in the spectrum of square wave with different duty ratios is different. With the increase of duty cycle, the energy concentrates to the low frequency band, and the transmission energy increases. In a certain frequency band, the uniformity of energy distribution decreases,

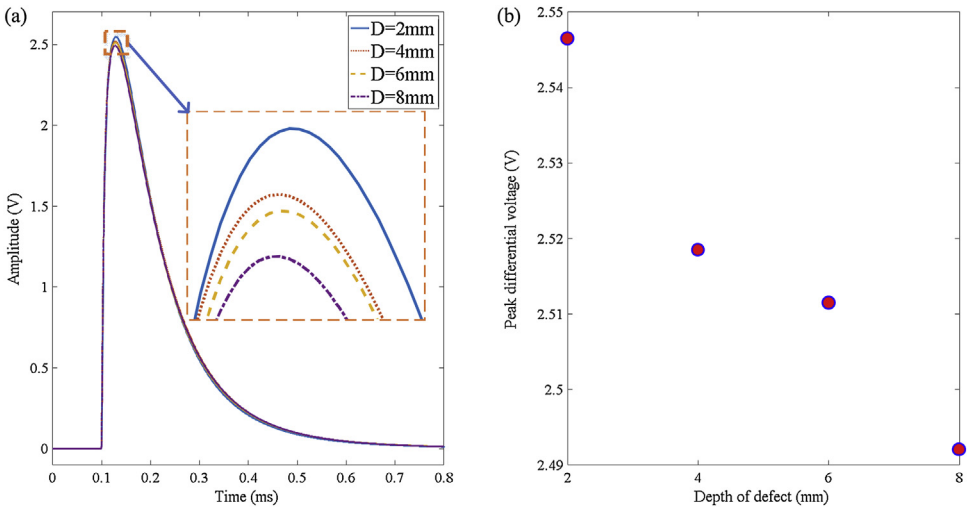

Fig. 10. The simulation response signal of different depth of defects on 45 steel. (a) Response signal, (b) The peak value of different defects.

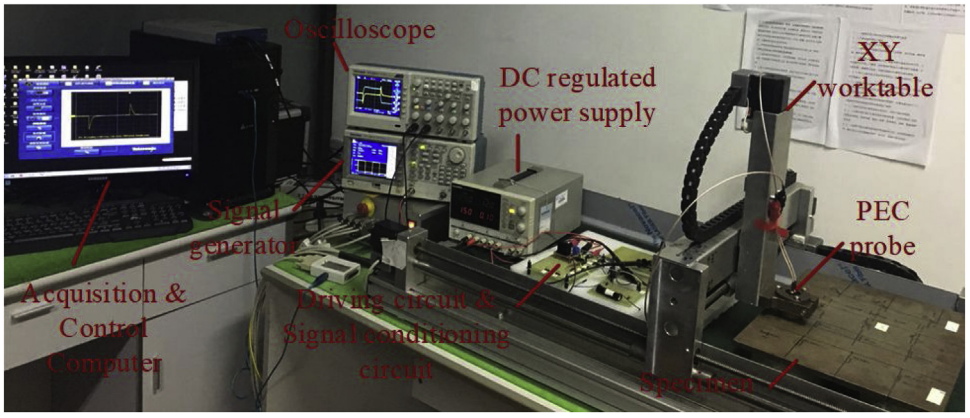

Fig. 11. Experiment setup with PEC probe.

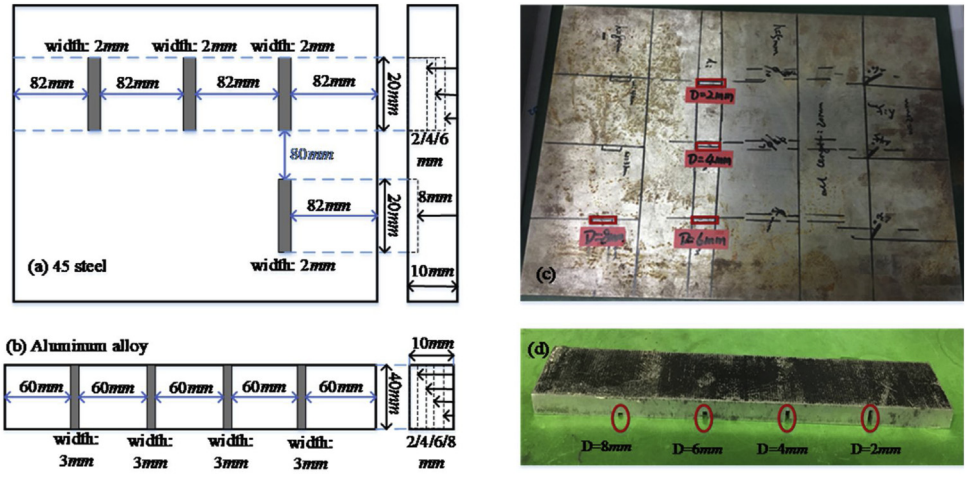

Fig. 12. Overview and side view of Defect on Samples. (a) Defects on 45 steel, (b) Defects on aluminum alloy, (c) Defect location on 45 Steel Specimen, (d) Defects location on aluminum alloy.

and it will affect the detection sensitivity. In addition, the detection sensitivity of the system can be optimized by selecting the proper equivalent impedance of the circuit. Notwithstanding above, when the excitation frequency is selected as a fixed value, it will cause the vibration of the specimen. Since the duty cycle is 40%, the resonance with the specimen is getting serious. Thus, the peak differential voltage at duty ratio 30% is smaller than those at duty ratio 20% and duty ratio 40% for the non-ferromagnetic materials. As shown in Fig. 13(e), the peak difference changes monotonically with defect depth for the duty cycles. In addition, the pulse signal with duty cycle of 50% promotes higher power, whereas its low frequency component portion decreases. In particular, the peak difference

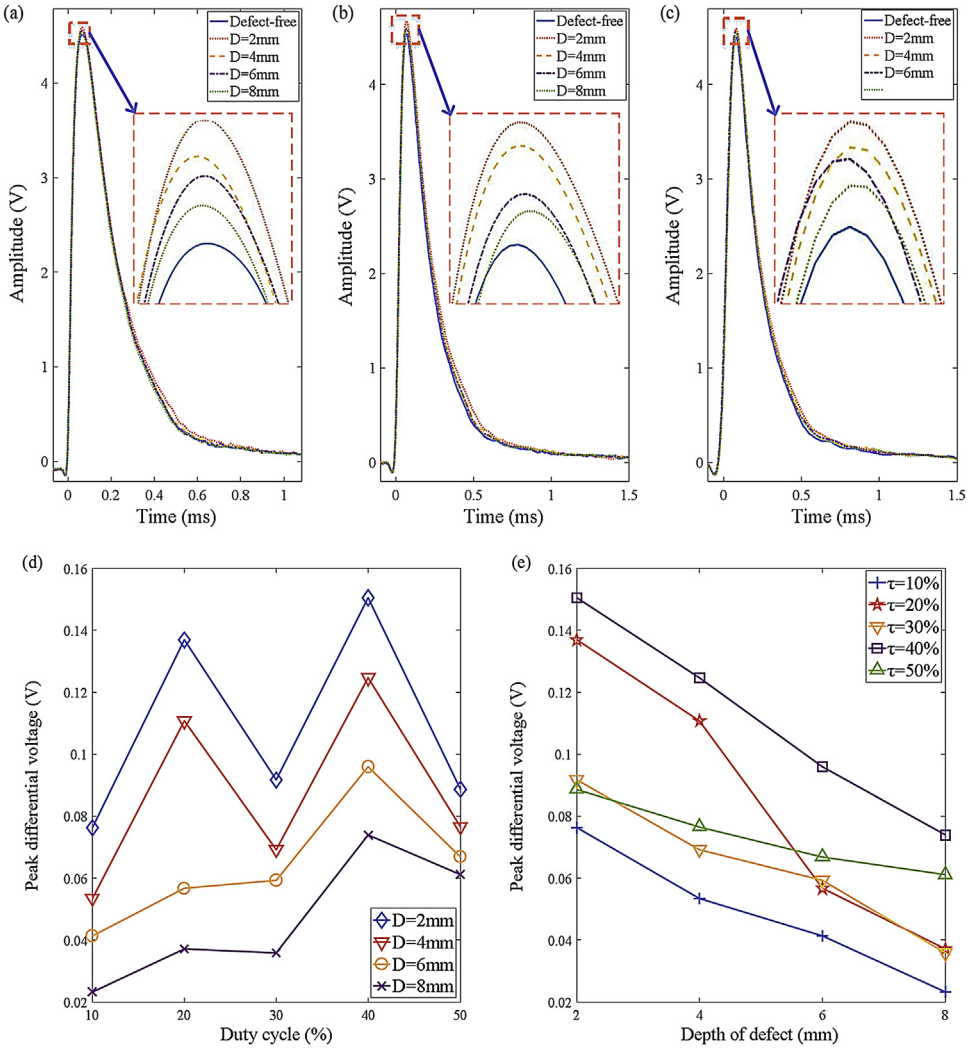

Fig. 13. The experimental response signal response signal of different depth of defects on aluminum alloy. (a) Response signal at τ = 10%, (b) Response signal at τ = 20%, (c) Response signal at τ = 30%, (d) Peak differential voltage with different duty cycle, (e) Peak differential voltage with different defect depths.

curve changes more slowly with the increase of defect depth. Thus, the ability to distinguish depth decreases. τ = 10% has the similar attenuation with τ = 30% and τ = 40%, however, its energy is weak and vulnerable to external interference. In general, τ = 40% is the best detection duty cycle, due to enough penetration depth and high energy. Moreover, τ = 20% is a better choice under the condition of distinguishing more defects with different depths.

The detected peak differential voltage of ferromagnetic materials is shown in Fig. 14. The response signals of τ = 10%, τ = 20% and τ = 30% are shown in Fig. 14(a)–(c), respectively. As shown in Fig. 14(d), τ = 10% has higher detection sensitivity due to its spectrum contains a higher portion of low-frequency components as this makes deeper penetration depth. In addition, the penetration depth is an important factor affecting the detection sensitivity of ferromagnetic material defect detection, and this feature is more prominent in the detection of ferromagnetic materials. From Fig. 14(e), the variation rate of peak difference is similar to that of different duty cycle. Compared with aluminum alloy specimens, the ability to distinguish the depth of defects is weak. Therefore, τ = 10% of deeper penetration depth is the optimal detection duty cycle.

The correlation coefficients between defect depth and sensitivity, duty cycle and defect depth are listed in Table 3. It can be seen that there is a significant negative correlation between defect depth and sensitivity.

In comparing the experimental response signal with the simulation response signal, it can be concluded that the experimental data and the simulation data retain the same trend of change. In addition, the variation of the peak characteristics with defect depth is monotonically correlated. This indicates that the proposed PEC structure based on weak coupling can effectively detect the deeply buried sub-surface defects.

4. Conclusion and future work

In this paper, a novel structure of the PEC probe based on weak coupling mechanism is proposed. Both simulation and verification experiments are conducted to validate its detection capability. Several conclusions can be drawn as follows: i). The proposed structure enables to improve the ratio of the indirect coupling energy to direct coupling energy and realize the deep defect information expression. ii). The proposed structure can correctly detect all subsurface defects for both ferromagnetic and non-ferromagnetic materials. iii). The influence of equivalent circuit and impedance on the response signal is analyzed. And both theoretical analysis and simulation results show that coil spacing is an important factor affecting the detection sensitivity directly and effectively.

In this paper, the peak value of the response signal can be considered as a feature to acquire more defect information in the early

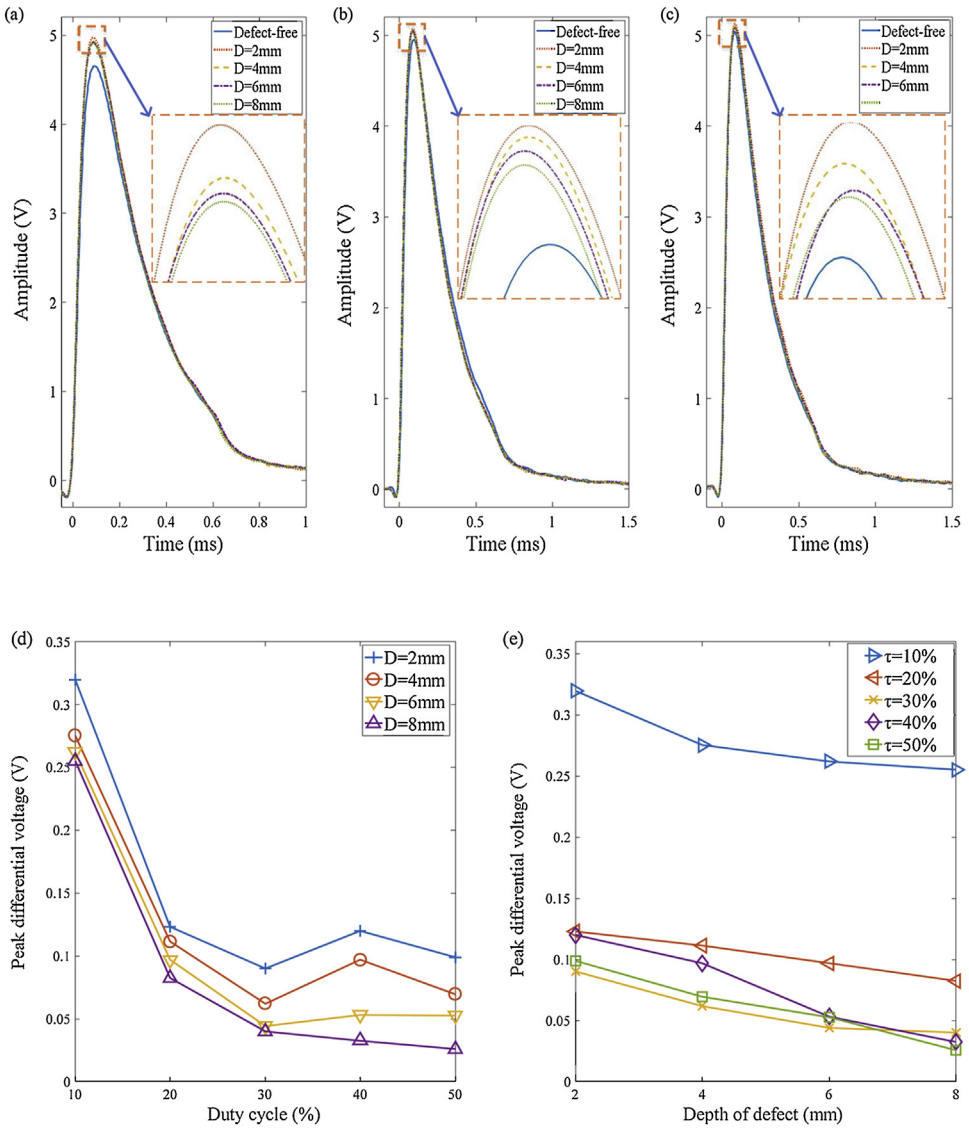

Fig. 14. The experimental response signal response signal of different depth of defects on 45 steel. (a) Response signal at τ = 10%, (b) Response signal at τ = 20%, (c) Response signal at τ = 30%, (d) Peak differential voltage with different duty cycle, (e) Peak differential voltage with different defect depths.

Table 3
Correlation coefficients between parameters of defect and sensitivity.

Parameter	Sensitivity (V)								Pearson Correlation Coefficients	
Specimen	aluminum alloy				45 steel				aluminum alloy	45 steel
Duty cycle τ (%)	Depth (*mm*)				Depth (*mm*)					
	2	4	6	8	2	4	6	8		
10	0.076	0.053	0.041	0.023	0.3198	0.2752	0.2621	0.255	−0.9933	−0.9206
20	0.137	0.111	0.057	0.037	0.123	0.111	0.097	0.082	−0.9838	−0.9989
30	0.092	0.069	0.059	0.036	0.09	0.062	0.044	0.04	−0.9897	−0.9527
40	0.151	0.125	0.096	0.074	0.119	0.097	0.053	0.033	−0.9987	−0.9898
50	0.089	0.077	0.067	0.061	0.099	0.069	0.053	0.026	−0.9881	−0.9954

stage of the attenuation period in the response signal. However, the feature is vulnerable to external interference. Research on the characteristic signal of pulse eddy current response for geometry sample should be involved in the future study.

Acknowledgement

The work was supported by state administration of quality supervision, inspection and quarantine (No. 2017QK042), supported by National Natural Science Foundation of China (No. 61401071, No. 61527803), supported by Science and Technology Department of Sichuan, China (Grant No.2018GZ0047)

References

[1] K. Song, Y.H. Kang, L.P. Zhang, Research progress in magnetic properties of steel pipe on the eddy current testing signal [J], J. Mater. Eng. 43 (11) (2015) 106–112.
[2] S. Obeid, F.M. Tranjan, T. Dogaru, Eddy current testing for detecting small defects in thin films[C]//, American Institute of Physics 894 (1) (2007) 340–345.

[3] N. Net, Detection of defect on Aircraft Multi-layered Structure by Eddy Current technique[J], Ndt Net (2014).
[4] Y. Kim, J.Y. Yi, S. Lee, Eddy current test of steel tube employing electromagnet technique for dc magnetization, J. Appl. Phys. 60 (9) (1986) 3327–3334.
[5] D. Rifai, A.N. Abdalla, N. Khamsah, et al., Subsurface defects evaluation using eddy current testing, Indian J. Sci.Technol. 9 (9) (2016) 1–7.
[6] Y. Yu, P. Du, Y. Liao, Study on effect of coil shape and geometric parameters on performance of eddy current sensor[J], Chinese J. Sci. Instru. 28 (6) (2007) 1045–1050.
[7] C.V. Dodd, W.E. Deeds, Absolute eddy-current measurement of electrical conductivity[C], Eddy Current Testing (1981).
[8] C. Wang, K. Wang, Z. Cong, et al., Eddy current testing on weld defect based on the dual frequency independent component analysis[C]// instrumentation and measurement technology Conference, IEEE (2017) 1–5.
[9] J. Kim, M. Le, J. Lee, et al., Eddy current testing and evaluation of Far-Side corrosion around rivet in jet-engine intake of aging supersonic aircraft, J. Nondestr. Eval. 33 (4) (2014) 471–480.
[10] H.T. Zhou, K. Hou, H.L. Pan, et al., Study on the optimization of eddy current testing coil and the defect detection sensitivity, Procedia Eng. 130 (2015) 1649–1657.
[11] M. Cao, W. Zhang, W. Zeng, et al., Research on the device of differential excitation type eddy current testing for metal defect detection[C]// nondestructive Evaluation/testing: New technology & application, IEEE (2013) 155–158.
[12] D. Zhou, J. Wang, J. Wu, et al., Investigation of rectangular differential probes for pulsed eddy current non-destructive testing, Insight - Non-Destructive Testing and Condition Monitoring 58 (2) (2016) 87–100.
[13] L. Shu, H. Songling, Z. Wei, et al., Improved immunity to lift-off effect in pulsed eddy current testing with two-stage differential probes, Russ. J. Nondestr. Test. 44 (2) (2008) 138–144.
[14] R. Grimberg, L. Udpa, A. Savin, et al., 2D eddy current sensor array, Ndt & E International 39 (4) (2006) 264–271.
[15] J. Kim, M. Le, J. Lee, et al., Eddy current testing and evaluation of Far-Side corrosion around rivet in jet-engine intake of aging supersonic aircraft, Journal of Nondestructive Evaluation 33 (4) (2014) 471–480.
[16] H.T. Wang, H.L. Sun, L.D. Cui, et al., Pulsed eddy current array imaging detection technology used for defect detection, Nondestructive Testing (8) (2010) 560–563.
[17] H. Huang, N. Sakurai, T. Takagi, et al., Design of an eddy-current array probe for crack sizing in steam generator tubes, Ndt & E Internat. 36 (7) (2003) 515–522.
[18] T. Kiwa, T. Kawata, H. Yamada, et al., Fourier-transformed eddy current technique to visualize cross-sections of conductive materials, Ndt E Internat. 40 (5) (2007) 363–367.
[19] Y. Li, B. Yan, D. Li, et al., Pulse-modulation eddy current inspection of subsurface corrosion in conductive structures[J], Ndt E Internat. 79 (2016) 142–149.
[20] W. Xiaozhi, Z. Honghui, L. Zhigang, Multi frequency eddy current detection of ceramic materials based on frequency modulation[J], J. Comput. Theor. Nanosci. 13 (issue 3) (2016) 1826–1830, 13(3):1826-1830.
[21] D. Zhou, M. Pan, X. Chang, et al., Research on detection modes of ferromagnetic component defects using pulsed eddy current[J], Chinese J. Sci. Instrum. (2017).
[22] A.K. Soni, B. Sasi, S. Thirunavukkarasu, et al., Development of eddy current probe for detection of deep sub-surface defects, Iete Techn. Rev. 33 (4) (2015) 386–395.
[23] S. Majidnia, J. Rudlin, R. Nilavalan, Investigations on a pulsed eddy current system for flaw detection using an encircling coil on a steel pipe, Insight-Non-Destructive Testing and Condition Monitoring 56 (10) (2014) 560–565 (6).
[24] D.F. He, M. Shiwa, Deep defect detection using eddy current testing with AMR sensor[J], PIERS Proc. 39 (4) (2013) 432–441.
[25] O. Hesse, S. Pankratyev, Usage of magnetic field sensors for low frequency eddy current testing, Measurement Sci. Rev. 5 (3) (2005) 86–93.
[26] R. Hohmann, M. Maus, D. Lomparski, et al., Aircraft wheel testing with machine-cooled HTS SQUID gradiometer system, IEEE Trans. Appl. Supercond. 9 (2) (1999) 3801–3804.
[27] M. Kreutzbruck, K. Allweins, C. Heiden, Fluxgate-magnetometer for the detection of deep lying defects, Proceedings of 15th WCNDT (2000).
[28] H.L. Kang, M.K. Baek, I.H. Park, Estimation of deep defect in ferromagnetic material by Low frequency eddy current method, IEEE Trans. Magn. 48 (11) (2012) 3965–3968.
[29] L. Janousek, Z. Chen, N. Yusa, et al., Excitation with phase shifted fields-enhancing evaluation of deep cracks in eddy-current testing, Ndt & E International 38 (6) (2005) 508–515.
[30] S. Majidnia, J. Rudlin, R. Nilavalan, A pulsed eddy current system for flaw detection using an encircling coil on a steel pipe, Insight - Non-Destructive Testing and Condition Monitoring 56 (10) (2014) 560–565 (6).
[31] C.S. Angani, D.G. Park, C.G. Kim, et al., Pulsed eddy current differential probe to detect the defects in a stainless steel pipe, J. Appl. Phys. 109 (7) (2011) 3455.
[32] G. Yang, A. Tamburrino, L. Udpa, et al., Pulsed eddy-current based giant magnetoresistive system for the inspection of aircraft structure, IEEE Trans. Magn. 46 (3) (2010) 910–917.
[33] Y. Li-Jian, P. Lei, Ji-Hua Y. Steel Pulsed, Eddy current testing method[J], Instrument Technique and Sensor 40 (7) (2011) 87–90.
[34] D.G. Park, C.S. Angani, B.P.C. Rao, et al., Detection of the subsurface cracks in a stainless steel plate using pulsed eddy current, J. Nondestr. Eval. 32 (4) (2013) 350–353.
[35] B. Lebrun, Y. Jayet, J.C. Baboux, Pulsed eddy current signal analysis: application to the experimental detection and characterization of deep flaws in highly conductive materials, NDT E Internat. 30 (3) (1997) 163–170.
[36] Y. He, M. Pan, F. Luo, et al., Pulsed eddy current imaging and frequency spectrum analysis for hidden defect nondestructive testing and evaluation, Ndt E Internat. 44 (4) (2011) 344–352.
[37] I.Z. Abidin, C. Mandache, G.Y. Tian, et al., Pulsed eddy current testing with variable duty cycle on rivet joints, NDT E Internat. 42 (7) (2009) 599–605.
[38] H.E. Xu, G.Z. Yan, M.A. Guan-Ying, Mutual inductance's affecting factors and its affection to the energy transmission efficiency of wireless energy transmission system[J], Measurement Control Technol. (2007).

Biographies

Lian Xie received the B.Sc. degree in Measurement and control technology and instrument from Southwest Petroleum University (2012–2016), Chengdu, China. She is currently pursuing the M.Sc. degree in nondestructive testing using eddy current technique at the University of Electronic Science and Technology of China, Chengdu, China. Her research interests include eddy current testing and wireless energy transfer.

Bin Gao received his B.Sc. degree in communications and signal processing from Southwest Jiao Tong University (2001–2005), China, MSc degree in communications and signal processing with Distinction and PhD degree from Newcastle University, UK (2006–2011). He worked as a Research Associate (2011–2013) with the same university on wearable acoustic sensor technology. Currently, he is a Professor with the School of Automation Engineering, University of Electronic Science and Technology of China (UESTC), Chengdu, China. His research interests include sensor signal processing, machine learning, social signal processing, nondestructive testing and evaluation where he actively publishes in these areas. He is also a very active reviewer for many international journals and long standing conferences. He has coordinated several research projects from National Natural Science Foundation of China.

Gui Yun Tian (M'01-SM'03) received the B.Sc. degree in metrology and instrumentation and M.Sc. degree in precision engineering from the University of Sichuan, Chengdu, China, in 1985 and 1988, respectively, and the Ph.D. degree from the University of Derby, Derby, U.K., in 1998. From 2000–2006, he was a Lecturer, Senior Lecturer, Reader, Professor, and Head of the group of Systems Engineering, respectively, with the University of Huddersfield, U.K. Since 2007, he has been based at Newcastle University, Newcastle upon Tyne, U.K., where he has been Chair Professor in Sensor Technologies. Currently, He is also an adjunct professor with School of Automation Engineering, University of Electronic Science and Technology of China. He has coordinated several research projects from the Engineering and Physical Sciences Research Council (EPSRC), Royal Academy of Engineering and FP7, on top of this he also has good collaboration with leading industrial companies such as Airbus, Rolls Royce, BP, nPower, Networkrail and TWI among others.

Jidong Tan is currently a M.S. engineer and working in China Special Equipment Testing Research Institute. He is engaged in non-destructive testing and evaluation of technical research. His main research interests include magnetic barkhausen, magnetic properties, magnetic multi-parameter detection method and other detection methods, sensors and detection equipment development.

Bo Feng received the B.Sc. degree in physics from Beijing Normal University, Beijing, China, in 2011, and the Ph.D. degree in measurement technology and instrumentation from the Huazhong University of Science and Technology, Wuhan, China, in 2016. He is currently a Post-Doctoral Researcher with the Instituto de Telecomunicações, Instituto Superior Técnico, Universidade de Lisboa, Lisbon, Portugal. His current research interests include electromagnetic non-destructive testing and guided ultrasonic wave testing.

Ying Yin received the BEng degree in Electrical Engineering from Xihua University in 2005, PhD degree in Digital Image Processing from Newcastle University in 2009. He is currently a Senior Engineer and Director of Research Department of Sichuan Special Equipment Inspection Institute. His major research includes non-destructive testing and evaluation for special equipment specifically, image processing.